Compositional Dependence of Phase Selection in CoCrCu$_{0.1}$FeMoNi-Based High-Entropy Alloys

Ning Liu [1,*] **, Chen Chen** [1] **, Isaac Chang** [2] **, Pengjie Zhou** [1] **and Xiaojing Wang** [1]

[1] School of Materials Science and Engineering, Jiangsu University of Science and Technology, Zhenjiang 212003, China; cc1870806525@163.com (C.C.); zhoupengjie@just.edu.cn (P.Z.); xjwang.0@163.com (X.W.)

[2] Brunel Centre for Advanced Solidification (BCAST), Brunel University, Kingston Lane, London UB8 3PH, UK; isaac.chang@brunel.ac.uk

* Correspondence: lnlynn@l26.com; Tel.: +86-511-8440-1184

check for
updates

Abstract: To study the effect of alloy composition on phase selection in the CoCrCu$_{0.1}$FeMoNi high-entropy alloy (HEA), Mo was partially replaced by Co, Cr, Fe, and Ni. The microstructures and phase selection behaviors of the CoCrCu$_{0.1}$FeMoNi HEA system were investigated. Dendritic, inter-dendritic, and eutectic microstructures were observed in the as-solidified HEAs. A simple face centered cubic (FCC) single-phase solid solution was obtained when the molar ratio of Fe, Co, and Ni was increased to 1.7 at the expense of Mo, indicating that Fe, Co, and Ni stabilized the FCC structure. The FCC structure was favored at the atomic radius ratio $\delta \leq 2.8$, valence electron concentration (VEC) ≥ 8.27, mixing entropy $\Delta S \leq 13.037$, local lattice distortion parameter $\alpha_2 \leq 0.0051$, and $\Delta S/\delta^2 > 1.7$. Mixed FCC + body centered cubic (BCC) structures occurred for $4.1 \leq \delta \leq 4.3$ and $7.71 \leq VEC \leq 7.86$; FCC or/and BCC + intermetallic (IM) mixtures were favored at $2.8 \leq \delta \leq 4.1$ or $\delta > 4.3$ and $7.39 < VEC \leq 8.27$. The IM phase is favored at electronegativity differences greater than 0.133. However, ΔS, α_2, and $\Delta S/\delta^2$ were inefficient in identifying the (FCC or/and BCC + IM)/(FCC + BCC) transition. Moreover, the mixing enthalpy cannot predict phase structures in this system.

Keywords: high-entropy alloy; microstructure; eutectic structure; phase selection

1. Introduction

High-entropy alloys (HEAs) represent a new class of materials that have attracted extensive attention since 2004 [1–8]. HEAs are defined as alloys containing at least five major elements wherein every major element has an atomic fraction between 5% and 35% [9]. Various studies on HEAs, including composition, processing, crystal structure and microstructure, and physical and mechanical properties, have been performed in the past years [5–23].

The microstructures and crystalline phases present in HEAs are very sensitive to the alloy composition. An α phase appears when the molar ratio of Mo in AlCoCrFeNiMo$_x$ alloys exceeds 0.1 [17]. Changes in the molar ratio of Fe, Co, and Cr in AlCoCrFeMo$_{0.5}$Ni alloys affect the crystalline phases and mechanical properties. As the Mo content increases, the volume fraction of the σ phase increases in Ni$_2$CrFeMo$_x$ alloys [18]. However, the volume fraction of the σ phase is increased with increasing Cr content. Eventually, the dendritic matrix of AlCoCr$_x$FeMo$_{0.5}$Ni HEAs is changed from the ordered B2 phase to the σ phase [19]. As the Co content in AlCo$_x$CrFeMo$_{0.5}$Ni HEAs changes from x = 0.5 to x = 2.0, the phase changes from BCC to BCC + FCC + σ, respectively. Recently, it was found that the precipitation of intermetallic (IM) compounds of σ and μ phases could strengthen CoCrFeNiMo$_{0.3}$ alloy without causing serious embrittlement [21]. Moreover, the ordered B2 solid-solution and σ phases were

presented in FeAlCrNiMo$_x$ HEAs with increasing Mo content [22]. Most previous investigations have focused on the effects of the addition or content change of one or two elements on the microstructure and properties of the HEA. However, studies on the effect of each individual element on the microstructure and phase selection have not yet been reported. Additional systematic research will be necessary in the near future to guide the exploration of HEAs.

Many parameters are related to phase selection in HEAs, including the atomic radii differences (δ), differences in electronegativity (ΔX), the valence electron concentration (VEC), the enthalpy of mixing (ΔH_{mix}), and the mixing entropy (ΔS_{mix}) [24–31]. Based on these parameters, many criteria have been proposed for phase prediction in HEAs. Zhang et al. summarized a solid-solution phase-forming rule using δ, ΔH_{mix}, and ΔS_{mix} with $\delta \leq 6.6\%$, $-22 \leq \Delta H_{mix} \leq 7$ kJ/mol, and $11 \leq \Delta S_{mix} \leq 19.5$ J/(K·mol) [24]. To limit the target of discussion to simple disordered phases, the conditions are more strict: $\delta \leq 4.3\%$, $-15 \leq \Delta H_{mix} \leq 5$ kJ/mol, and $12 \leq \Delta S_{mix} \leq 17.5$ J/(K·mol). Guo proposed that the phase stability of the FCC and BCC solid solution was correlated with VEC; for VEC < 6.87 the BCC phase was stable; for VEC > 8, FCC was [25]. Later, the stability of the σ phase was studied and it was predicted that alloys with $6.88 \leq$ VEC ≤ 7.84 were prone to σ phase formation [30]. However, this criterion works well only for Cr- and V-containing HEAs. Recently, complex ordered phases were found to be stable for $\Delta X > 0.133$, except for HEAs containing a large amount of Al [31]. More recently, Wang et al. [32] proposed a new parameter, α_2, to address the local lattice distortion of crystalline lattices in HEAs. This parameter effectively explained the lattice distortion, intrinsic strain energy, and excess entropy in HEAs.

As mentioned above, the phases present in HEAs are remarkably dependent on the alloy composition. In a previous work, the CoCrCu$_{0.1}$FeMoNi alloy exhibited the duplex microstructure of BCC + FCC [33]. Under compositional change, the microstructural behavior is uncertain: the HEA could retain this simple solid solution mixture or intermetallic (IM) phases could appear. In order to address this question, it is necessary to study the effect of alloy composition on the phase selection of CoCrCu$_{0.1}$FeMoNi alloys. Hence, the present work investigates the partial substitution of Mo by Cr, Co, Ni, and Fe. The effect of the relative contents of Cr, Co, Ni, Fe, and Mo on the microstructure and crystal structures of CoCrCu$_{0.1}$FeMoNi-based HEAs was studied in this work in order to understand the phase selection mechanism in this alloy system.

2. Materials and Methods

The proposed HEAs were prepared via vacuum arc melting in a Ti-gettered Ar atmosphere with subsequent melt solidification in a water-cooled Cu crucible. A mixture of the appropriate amounts of the constituent elements with purities > 99.9 wt % for each alloy was flipped and melted at least four times to ensure thorough chemical homogeneity. Table 1 shows the compositions prepared in this study. As-cast samples were then sectioned and polished for microstructural and compositional characterization using scanning electron microscopy (SEM, JEOL-5410, JEOL Ltd., Tokyo, Japan), energy dispersive X-ray spectrometry (EDS, JEOL Ltd., Tokyo, Japan), and an X-ray diffractometer (XRD, Rigaku ME510-FM2, Rigaku Ltd., Tokyo, Japan) at a scanning speed of 4°/min and a scanning range from 30° to 100° using a Cu target and an applied voltage and current of 30 kV and 20 mA, respectively.

Table 1. A list of chemical composition of CoCrCu$_{0.1}$FeMoNi-based alloys (at %).

Alloys	Co	Cr	Cu	Fe	Mo	Ni
Co$_{1.2}$CrCu$_{0.1}$FeMo$_{0.8}$Ni	23.53	19.61	1.96	19.61	15.69	19.61
Co$_{1.5}$CrCu$_{0.1}$FeMo$_{0.5}$Ni	29.41	19.61	1.96	19.61	9.8	19.61
Co$_{1.7}$CrCu$_{0.1}$FeMo$_{0.3}$Ni	33.33	19.61	1.96	19.61	5.88	19.61
CoCr$_{1.2}$Cu$_{0.1}$FeMo$_{0.8}$Ni	19.61	23.53	1.96	19.61	15.69	19.61
CoCr$_{1.5}$Cu$_{0.1}$FeMo$_{0.5}$Ni	19.61	29.41	1.96	19.61	9.8	19.61
CoCrCu$_{0.1}$Fe$_{1.2}$Mo$_{0.8}$Ni	19.61	19.61	1.96	23.53	15.69	19.61
CoCrCu$_{0.1}$Fe$_{1.5}$Mo$_{0.5}$Ni	19.61	19.61	1.96	29.41	9.8	19.61
CoCrCu$_{0.1}$Fe$_{1.7}$Mo$_{0.3}$Ni	19.61	19.61	1.96	33.33	5.88	19.61
CoCrCu$_{0.1}$Fe Mo$_{0.8}$Ni$_{1.2}$	19.61	19.61	1.96	19.61	15.69	23.53
CoCrCu$_{0.1}$Fe Mo$_{0.5}$Ni$_{1.5}$	19.61	19.61	1.96	19.61	9.8	29.41
CoCrCu$_{0.1}$Fe Mo$_{0.3}$Ni$_{1.7}$	19.61	19.61	1.96	19.61	5.88	33.33

3. Results

3.1. Co$_a$CrCu$_{0.1}$FeMo$_{2-a}$Ni Alloys

The microstructures of the Co$_a$CrCu$_{0.1}$FeMo$_{2-a}$Ni (a = 1.2, 1.5 and 1.7) alloys are shown in Figure 1. A typical eutectic structure is found in the inter-dendritic region, and the volume fraction of the eutectic mixture is decreased with increasing Co and decreasing Mo. Table 2 shows the actual composition and contents of different regions in the microstructures, as detected by EDS. The dendrites are enriched in Co, Cu, Fe, and Ni, while the contents of Cr and Mo are higher in the inter-dendritic region B. The composition of the inter-dendritic eutectic region B is approximately (CrMo)$_{54}$(CoCuFeNi)$_{46}$ according to EDS. This means that the content of Cr and Mo is 54% and that of Co, Cu, Fe, and Ni is 46%. Furthermore, the Cu content in the inter-dendritic region is increased with decreasing Mo content. This is related to the positive ΔH_{mix} between Cu and Mo (+19 kJ/mol).

Figure 1d shows the XRD patterns of the Co$_a$CrCu$_{0.1}$FeMo$_{2-a}$Ni HEAs. The FCC, σ, and μ phases are detected. The crystal structure of the σ phase is tetragonal with the lattice constants of a = 0.885 nm and c = 0.459 nm, and the σ phase is similar to the binary Co$_2$Mo$_3$ phase. The μ phase is tetragonal with lattice constants of a = 0.7381 nm and c = 1.8504 nm, and probably Co$_7$Mo$_3$ or Fe$_7$Mo$_6$. Both σ and μ are topologically close-packed (TCP) phases. Obviously, the volume fractions of the σ and μ phases, represented by peaks in the range of 40–50°, are decreased as the Co content increases and Mo decreases. According to the EDS and XRD results, we can identify the dendrites as the FCC phase, while σ and μ are eutectic structures.
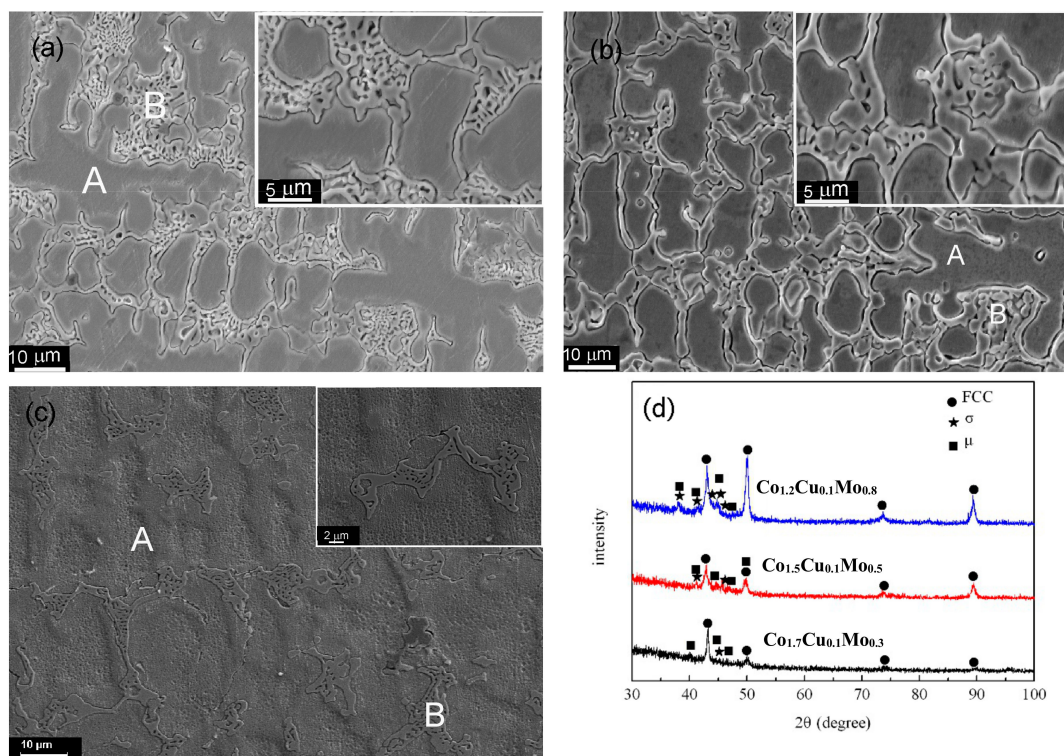
Figure 1. The microstructures and phases of Co$_a$CrCu$_{0.1}$FeMo$_{2-a}$Ni HEAs. (**a**) Co$_{1.2}$CrCu$_{0.1}$FeMo$_{0.8}$Ni; (**b**) Co$_{1.5}$CrCu$_{0.1}$FeMo$_{0.5}$Ni; (**c**) Co$_{1.7}$CrCu$_{0.1}$FeMo$_{0.3}$Ni; (**d**) X-ray diffractometer (XRD) patterns.

Table 2. The components of different regions in microstructures of $CoCrCu_{0.1}FeMoNi$-based high-entropy alloys (HEAs).

Alloy	Value	Region	Co	Cr	Cu	Fe	Mo	Ni
$Co_aCrCu0.1FeMo_{2-a}Ni$	$a = 1.2$	Content	23.55	18.37	1.84	19.73	17.93	18.58
		A	24.17	18.46	1.85	20.45	14.32	20.75
		B	19.32	18.01	0.43	14.57	36.10	11.57
	$a = 1.5$	Content	27.92	20.60	1.8	19.63	9.5	19.55
		A	20.45	27.40	1.68	21.25	8.93	20.29
		B	17.03	33.13	0.82	16.70	19.91	12.41
	$a = 1.7$	Content	33.63	19.57	1.75	19.8	6.00	19.25
		A	34.86	17.83	1.61	20.30	6.09	19.31
		B	30.34	20.33	1.90	19.79	8.98	18.66
$CoCr_bCu0.1FeMo_{2-b}Ni$	$b = 1.2$	Content	19.32	25.69	1.85	20.44	12.36	20.34
		A	18.68	30.11	-	20.20	9.53	21.47
		B	22.51	22.99	1.77	17.02	17.53	18.17
	$b = 1.5$	Content	20.02	29.45	1.51	19.23	10.36	19.43
		A	15.50	26.95	-	18.31	24.98	14.25
		B	16.76	24.25	-	19.83	19.13	20.03
$CoCrCu0.1Fe_cMo_{2-c}Ni$	$c = 1.2$	Content	15.33	21.76	1.83	23.53	17.92	19.63
		A	15.70	21.66	-	20.57	29.21	12.86
		B	14.95	22.12	0.40	20.93	29.95	11.65
	$c = 1.5$	Content	17.71	21.65	1.94	29.41	10.82	18.47
		A	17.63	19.24	2.25	31.42	10.49	18.95
		B	15.51	21.98	0.34	23.16	27.19	11.83
		C	15.94	22.96	0.62	22.66	24.96	12.85
	$c = 1.7$	Content	20.8	19.98	1.64	33.30	6.05	18.23
		A	18.95	19.89	1.58	32.19	8.45	18.94
		B	22.54	20.36	1.89	34.23	2.81	18.16
$CoCrCu0.1FeMo_{2-d}Ni_d$	$d = 1.2$	Content	19.37	19.63	1.36	19.47	16.64	23.53
		A	19.49	18.93	1.20	21.82	13.50	25.06
		B	16.80	22.33	0.67	16.58	27.68	15.95
		C	17.03	21.79	0.45	13.97	32.56	14.20
	$d = 1.5$	Content	19.79	19.68	1.96	19.16	10.37	29.04
		A	19.09	19.13	2.15	17.77	13.22	28.65
		B	21.82	20.07	1.71	21.02	3.28	32.10
		C	18.28	22.86	0.67	15.67	21.82	20.70
	$d = 1.7$	Content	20.82	19.67	1.53	19.74	6.25	31.89
		A	17.80	21.90	1.84	18.78	8.06	31.62
		B	21.38	19.25	1.65	19.93	4.60	33.18
		C	2.44	88.74	-	3.85	0.68	4.29

3.2. $CoCr_bCu_{0.1}FeMo_{2-b}Ni$ Alloys

The microstructures of $CoCr_bCu_{0.1}FeMo_{2-b}Ni$ ($b = 1.2$ and 1.5) alloys are shown in Figure 2. Dendrites and inter-dendritic regions remain in the $CoCr_{1.2}Cu_{0.1}FeMo_{0.8}Ni$ alloy (referred to as $Cr_{1.2}Cu_{0.1}Mo_{0.8}$). The dendrites are enriched in Fe and Ni, and the Cr content in the dendrites is increased (A in Figure 2a), while the inter-dendritic region (B) is enriched with Co and Mo. However, for the $CoCr_{1.5}Cu_{0.1}FeMo_{0.5}Ni$ alloy (referred to as $Cr_{1.5}Cu_{0.1}Mo_{0.5}$), a fully eutectic structure is found, indicating that the alloy has a eutectic composition, probably of $(CrMo)_{52}(CoCuFeNi)_{48}$, according to region A in Table 2 as detected by EDS. This means that the content of Cr and Mo is 52%, and that of Co, Cu, Fe, and Ni is 48%.

It is apparent that $CoCr_bCu_{0.1}FeMo_{2-b}Ni$ ($b = 1.2$ and 1.5) alloys contain FCC, BCC, and TCP phases according to the XRD patterns, as shown in Figure 2c. The TCP phases correspond to the tetragonal σ phase

(a = 0.917 nm, c = 0.474 nm) and a hexagonal close-packed (HCP) Laves phase (a = 0.473 nm, c = 0.772 nm). As can be seen in Figure 2c, the volume fraction of the BCC phase increases with increasing Cr, which enhances the formation of BCC phase in $CoCr_bCu_{0.1}FeMo_{2-b}Ni$ alloys (b = 1.2 and 1.5). With increasing Cr and decreasing Mo, the BCC phase appears, and the volume fraction of both TCP phases decreases. According to the EDS and XRD results, the dendrites should be FCC, while the eutectic structures include BCC, σ, and Laves phases.
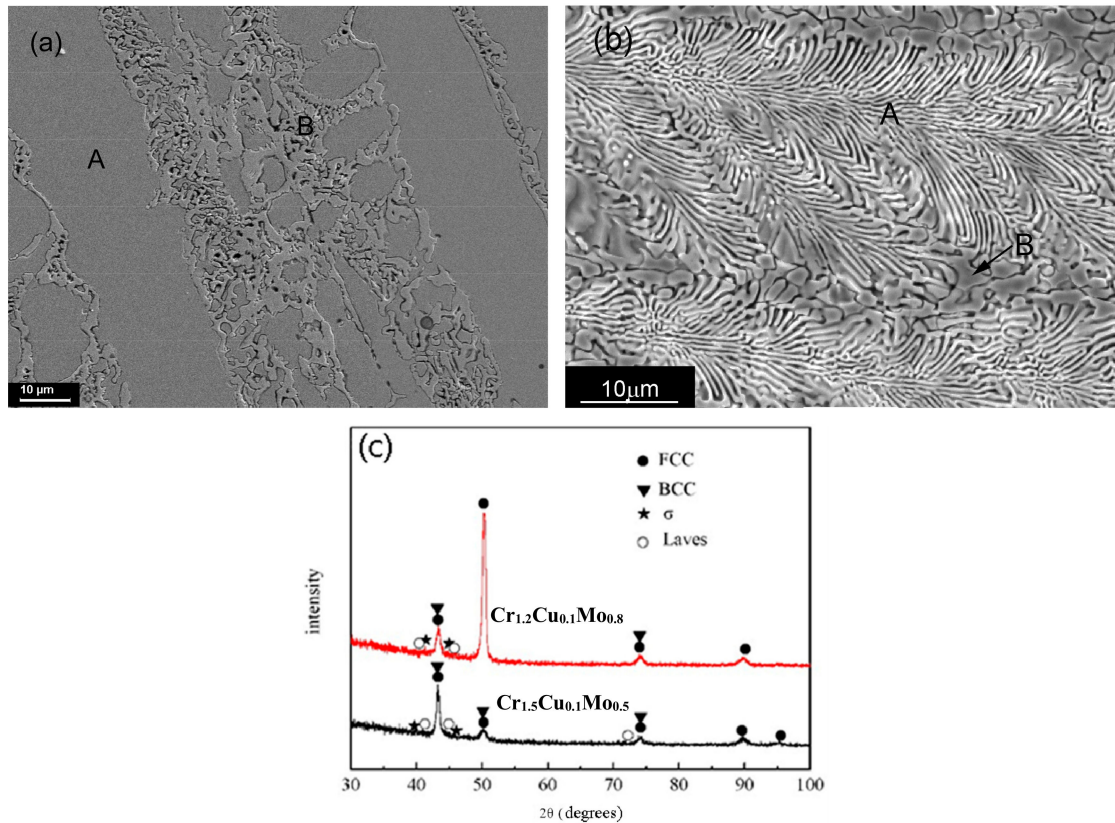
Figure 2. The SEM micrographs and phase structures of $CoCr_bCu_{0.1}FeMo_{2-b}Ni$ alloys. (**a**) $CoCr_{1.2}Cu_{0.1}FeMo_{0.8}Ni$; (**b**) $CoCr_{1.5}Cu_{0.1}FeMo_{0.5}Ni$; (**c**) XRD patterns.

3.3. $CoCrCu_{0.1}Fe_cMo_{2-c}Ni$ Alloys

Figure 3 presents the microstructures of the $CoCrCu_{0.1}Fe_cMo_{2-c}Ni$ (c = 1.2, 1.5 and 1.7) HEAs. A fully eutectic structure is obtained in the $CoCrCu_{0.1}Fe_{1.2}Mo_{0.8}Ni$ alloy (referred to as $Cu_{0.1}Fe_{1.2}Mo_{0.8}$). As shown in Table 2, the composition of the eutectic region is approximately $(CrMo)_{51}(CoCuFeNi)_{49}$. Similar to the $Co_{1.5}Cu_{0.1}Mo_{0.5}$ and $Co_{1.7}Cu_{0.1}Mo_{0.3}$ alloys, the microstructures of the $CoCrCu_{0.1}Fe_{1.5}Mo_{0.5}Ni$ (referred to as $Cu_{0.1}Fe_{1.5}Mo_{0.5}$) and $CoCrCu_{0.1}Fe_{1.7}Mo_{0.3}Ni$ (referred to as $Cu_{0.1}Fe_{1.7}Mo_{0.3}$) alloys comprise dendritic and inter-dendritic regions. The volume fraction of the inter-dendritic eutectic region decreases dramatically with increasing Fe and decreasing Mo contents. The dendrites (region A) of the $Cu_{0.1}Fe_{1.5}Mo_{0.5}$ alloy is enriched in Co, Cu, Fe, and Ni; the content of Cr and Mo is higher in the inter-dendritic regions B and C. Region A of the $Cu_{0.1}Fe_{1.7}Mo_{0.3}$ alloy is enriched in Mo; the content of Cu, Co, and Fe is higher in region B; and the contents of Cr and Ni are almost the same.

The XRD patterns of the $CoCrCu_{0.1}Fe_cMo_{2-c}Ni$ (c = 1.2, 1.5, 1.7) HEAs are shown in Figure 3d. FCC, μ (Fe_7Mo_3), and Laves phases are found in these alloys. The μ phase is trigonal (a = 0.7381 nm, c = 18.504 nm) and the Laves phase is HCP with a = 0.473 nm and c = 0.772 nm). Based on the intensities of the diffraction peaks, decreased Mo and increased Fe contents yield decreases in the volume fractions of the μ and Laves phases and increases in that of the FCC phase. For the $Cu_{0.1}Fe_{1.2}Mo_{0.8}$ alloy, the FCC, μ, and Laves phases form a eutectic structure. For the $Cu_{0.1}Fe_{1.5}Mo_{0.5}$

alloy, region A is FCC, region B should be the μ (Fe_7Mo_3) phase, and region C is probably FCC. For the $Cu_{0.1}Fe_{1.7}Mo_{0.3}$ alloy, both region A and B are FCC structures with different contents.
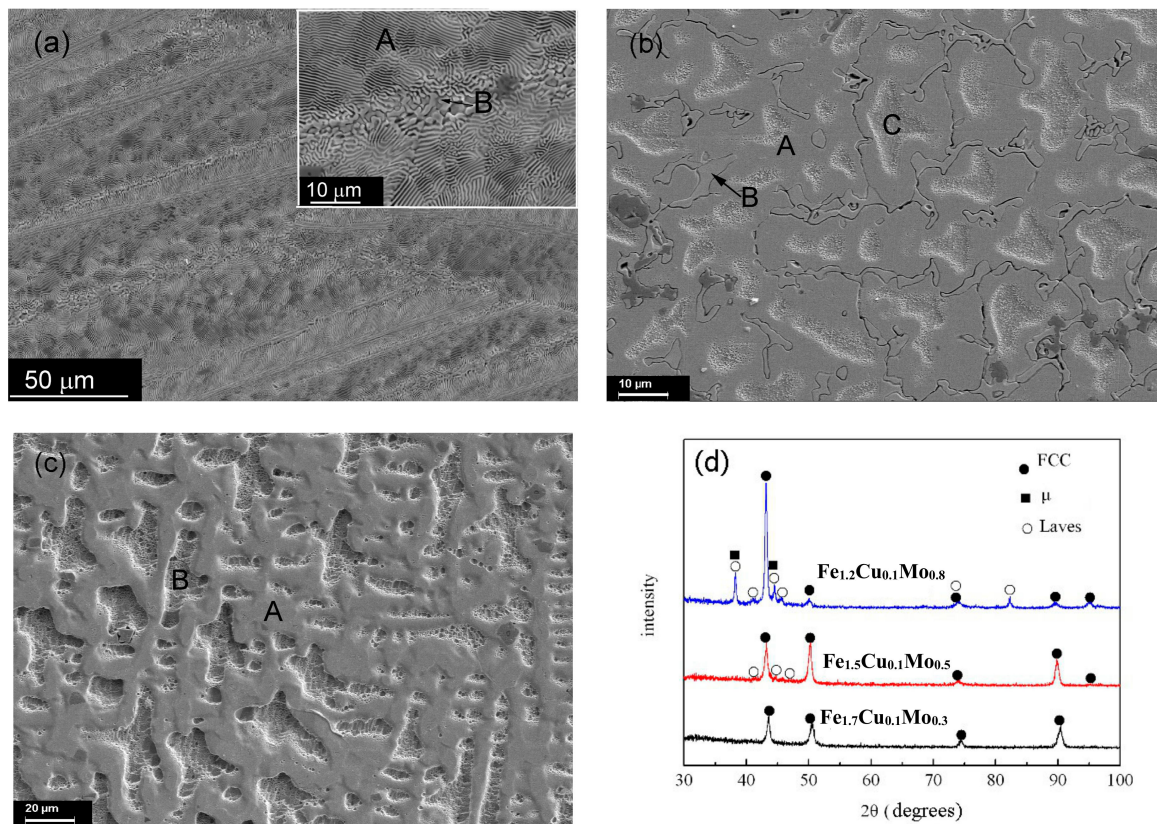
Figure 3. Micrographs and XRD patterns of $CoCrCu_{0.1}Fe_cMo_{2-c}Ni$ HEAs: (**a**) $Cu_{0.1}Fe_{1.2}Mo_{0.8}$; (**b**) $Cu0.1Fe_{1.5}Mo_{0.5}$; (**c**) $Cu_{0.1}Fe_{1.7}Mo_{0.3}$; (**d**) XRD patterns.

3.4. CoCrCu_{0.1}FeMo_{2−d}Ni_d Alloys

A similar microstructure, consisting of a dendritic matrix and inter-dendritic regions, is found in $CoCrCu_{0.1}FeMo_{2-d}Ni_d$ (d = 1.2, 1.5 and 1.7) HEAs, as shown in Figure 4. For the $Cu_{0.1}Mo_{0.8}Ni_{1.2}$ alloy, the dendrites are enriched in Co, Cu, Fe, and Ni (Region A in Figure 4a), while the inter-dendritic region (B) is enriched with Cr and Mo. The composition of the eutectic region is found to be approximately $(CrMo)_{54}(CoCuFeNi)_{46}$, as shown in Table 2. For the $Cu_{0.1}Mo_{0.5}Ni_{1.5}$ alloy, region A is enriched in Cu and Mo, region B has a higher content of Cr, Co, Fe, and Ni, and region C is enriched with Cr and Mo. Many flower-like structures with four petals (labeled C) are observed in the $Cu_{0.1}Mo_{0.3}Ni_{1.7}$ alloy; these structures are enriched with Cr.

The XRD results demonstrate that the alloys contain a trigonal μ phase (a = 0.7381 nm, c = 18.504 nm), FCC phase, and a small amount of an HCP Laves phase (a = 0.473 nm, c = 0.772 nm), as can be seen in Figure 4d. When the molar ratio of Ni is increased to 1.7, only the FCC phase is found in the solidified microstructure. Thus, it is demonstrated that Ni promotes the formation of the FCC phase. For the $Cu_{0.1}Mo_{0.8}Ni_{1.2}$ alloy, FCC is the dendritic phase, while the μ and Laves phases form a eutectic structure. For the $Cu_{0.1}Mo_{0.5}Ni_{1.5}$ alloy, both regions A and B are FCC structures, and region C should be the μ phase. For the $Cu_{0.1}Mo_{0.3}Ni_{1.7}$ alloy, both regions A and B are FCC structures with different contents, while region C is an unknown Cr-rich phase that cannot be detected because of its small amount.
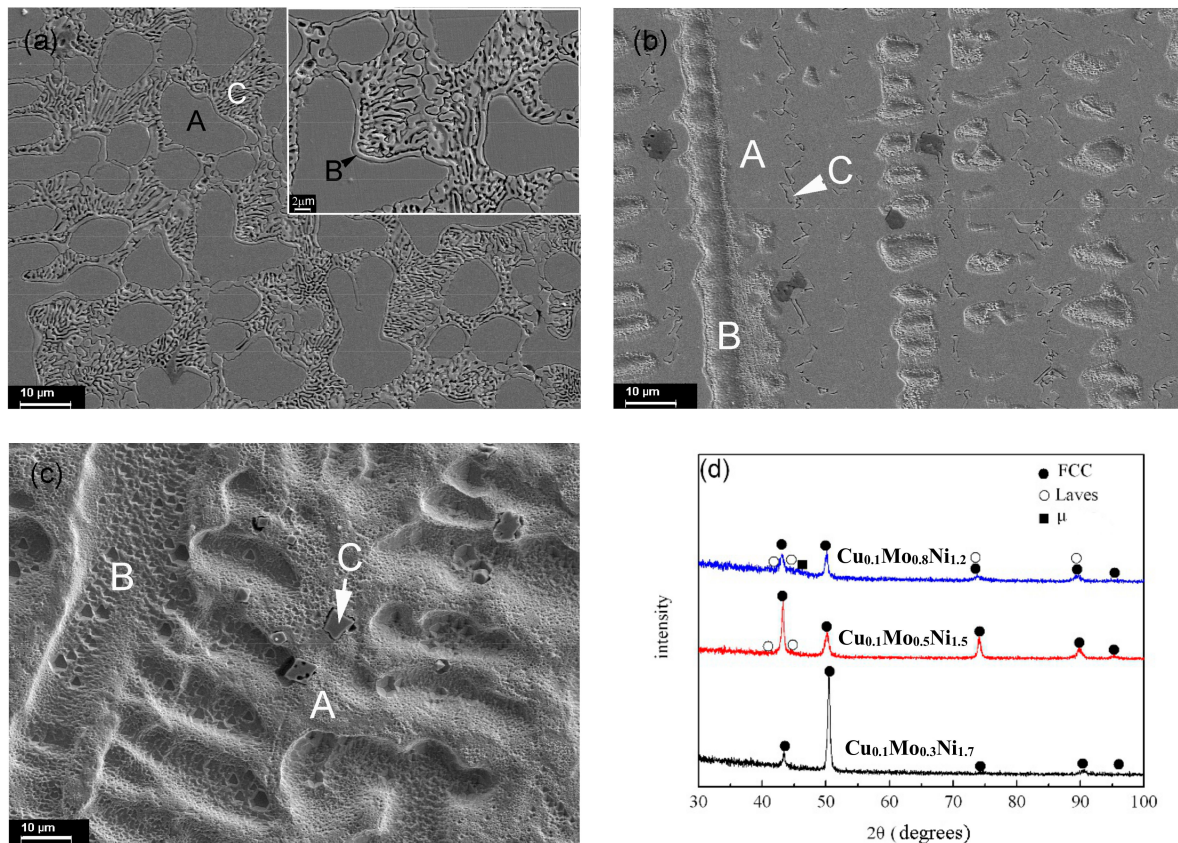
Figure 4. Microstructures and XRD patterns of the $CoCrCu_{0.1}FeMo_{2-d}Ni_d$ HEAs. (**a**) $Cu_{0.1}Mo_{0.8}Ni_{1.2}$; (**b**) $Cu_{0.1}Mo_{0.5}Ni_{1.5}$; (**c**) $Cu_{0.1}Mo_{0.3}Ni_{1.7}$; (**d**) XRD patterns.

4. Discussion

Two eutectic phases are found in the $Cr_{1.5}Cu_{0.1}Mo_{0.5}$ and $Cu_{0.1}Fe_{1.2}Mo_{0.8}$ HEAs, with probable eutectic compositions of $(CrMo)_{51-54}(CoCuFeNi)_{46-49}$. Similarly, fully eutectic structures have been obtained in $CoFeNi_xVMo_y$ HEAs at both $CoFeNi_{1.4}VMo$ and $CoFeNiVMo_{0.6}$ [14]. Recently, Lu et al. [34] have proposed a strategy to design eutectic high-entropy alloys (EHEAs) based on ΔH_{mix}. They selected Zr, Nb, Hf, and Ta to replace Al in a previous $AlCoCrFeNi_{2.1}$ EHEA, based on the relationship of ΔH_{mix} for various atomic pairs. Unfortunately, no regularities have yet been found in the current HEA system. Further research is ongoing to clarify this relationship in the future.

The phase selection mechanism in the $CoCrCu_{0.1}FeMoNi$-based HEAs can be understood using the parameters listed in Table 3. Based on alloy composition, a simple FCC structure is obtained only when the $CoCrCu_{0.1}FeMoNi$-based HEAs contain higher contents of principal elements, such as Fe/Co/Ni. This suggests that Fe, Co, and Ni are FCC stabilizers in the $CoCrCu_{0.1}FeMoNi$-based alloys. It can be found that a simple FCC structure is favorable for alloys with the smallest δ, ΔX, and ΔS. Conversely, alloys with large VEC values favor the formation of simple FCC structures, while TCP phases develop in alloys with smaller VEC values. TCP phases are found when the ΔH of the alloys is largely negative, with the exception of $Cu_{0.1}Mo_{0.3}Ni_{1.7}$. Furthermore, alloys with small α_2 favor the formation of a single-phase FCC structure. In the current work, the FCC structure is stable when $\delta \leq 2.8$, FCC+BCC is favored when $4.1 \leq \delta \leq 4.3$, and FCC or/and BCC + IM is found when $2.8 \leq \delta \leq 4.1$ or $\delta > 4.3$, with the only exception of $AlCoCrCuFeNiMo_{0.2}$. As shown in Figure 5c, the FCC structure is stable when VEC ≥ 8.27, but there is an overlap between the mixture types of FCC+BCC and FCC or/and BCC + IM. The IM phase is favored when $\Delta X > 0.133$ only with the exceptions of the $CoCrCu_{0.1}FeMoNi$ and $CoCrCu_{0.3}FeMoNi$ alloys.

The results are well fitted with the criterion proposed by Lu et al. As shown in Figure 5b,f, the FCC structure is stable when $\Delta S \leq 13.037$ and $\alpha_2 \leq 0.0051$; however, the (FCC+BCC)-type phase-forming ΔS and α_2 ranges show overlaps with those of the (FCC or/and BCC + IM)-type. All the calculated values of ΔH are in the range $-15 \leq \Delta H_{mix} \leq 5$ kJ/mol (Figure 5a), and except for FCC and BCC, IM phases are still found, indicating that the phase structures of the listed alloys cannot be distinguished by ΔH.

Singh demonstrated that a simple solid solution as obtained when $\Delta S_{mix}/\delta^2 > 0.96$, IM compounds when $\Delta S_{mix}/\delta^2 < 0.24$, and a mixture thereof when $0.24 < \Delta S_{mix}/\delta^2 < 0.96$ [36]. As can be seen in Figure 5e, a large $\Delta S/\delta^2$ value favors the formation of a single FCC phase. As the value of $\Delta S/\delta^2$ decreases, more phases appear, and smaller $\Delta S/\delta^2$ values favor the BCC phase. For $CoCrCu_{0.1}FeMoNi$-based alloys, the simple FCC phase structure is favored when $\Delta S/\delta^2 > 1.7$, while multiphase structures containing (FCC or/and BCC + IM) are found when $0.549 \leq \Delta S/\delta^2 \leq 1.28$, and the (FCC+BCC)-type phase-forming $\Delta S/\delta^2$ range shows an overlap with that of the (FCC or/and BCC + IM)-type. The former famous criterion for phase-forming in HEAs cannot be used effectively in this system. Thus, new rules or parameters must be considered in the future.

Table 3. Phases and parameters of $CoCrCu_{0.1}FeMoNi$-based HEAs.

Alloy	δ (%)	VEC	ΔX	ΔH (kJ·mol^{-1})	ΔS (J·K^{-1}·mol^{-1})	α_2	$\Delta S/\delta^2$	Phases	Ref.
$Co_{1.2}CrCu_{0.1}FeMo_{0.8}Ni$	3.912	7.977	0.150	−0.878	13.853	0.0089	0.9052	FCC + σ + μ	
$Co_{1.5}CrCu_{0.1}FeMo_{0.5}Ni$	3.291	8.154	0.132	−0.807	13.492	0.0070	1.2457	FCC + σ + μ	
$Co_{1.7}CrCu_{0.1}FeMo_{0.3}Ni$	2.705	8.271	0.118	−0.740	13.037	0.0051	1.7817	FCC	
$CoCr_{1.2}Cu_{0.1}FeMo_{0.8}Ni$	3.882	7.860	0.156	−0.897	13.853	0.0097	0.9192	FCC + BCC + Laves	
$CoCr_{1.5}Cu_{0.1}FeMo_{0.5}Ni$	3.247	7.860	0.145	−0.882	13.492	0.0069	1.2797	FCC + BCC + σ + Laves	
$CoCrCu_{0.1}Fe_{1.2}Mo_{0.8}Ni$	3.900	7.938	0.150	−0.847	13.853	0.0097	0.9108	FCC + Laves + Fe_7Mo_3	
$CoCrCu_{0.1}Fe_{1.5}Mo_{0.5}Ni$	3.260	8.056	0.132	−0.745	13.492	0.0069	1.2695	FCC + Laves	
$CoCrCu_{0.1}Fe_{1.7}Mo_{0.3}Ni$	2.669	8.314	0.117	−0.670	13.037	0.0045	1.8301	FCC	
$CoCrCu_{0.1}FeMo_{0.8}Ni_{1.2}$	3.933	8.016	0.150	−0.923	13.853	0.0089	0.8956	FCC + Laves + Fe_7Mo_3	
$CoCrCu_{0.1}FeMo_{0.5}Ni_{1.5}$	3.339	8.252	0.133	−0.907	13.492	0.0070	1.2102	FCC + Laves	
$CoCrCu_{0.1}FeMo_{0.3}Ni_{1.7}$	2.768	8.408	0.119	−0.869	13.037	0.0051	1.7016	FCC	
$Al_{0.1}CoCrCu_{0.1}FeMo_{0.9}Ni$	4.35	7.80	0.159	−1.116	14.45	0.0367	0.7636	FCC + Laves	[35]
$Al_{0.2}CoCrCu_{0.1}FeMo_{0.8}Ni$	4.48	7.74	0.158	−1.322	14.73	0.0405	0.7339	FCC + BCC + Laves + σ	[35]
$Al_{0.3}CoCrCu_{0.1}FeMo_{0.7}Ni$	4.61	7.68	0.157	−1.523	14.91	0.0417	0.7016	FCC + BCC + Laves + σ	[35]
$Al_{0.5}CoCrCu_{0.1}FeMo_{0.5}Ni$	4.85	7.57	0.151	−1.915	15.05	0.0449	0.6398	FCC + BCC+ Laves + σ	[35]
$Al_{0.8}CoCrCu_{0.1}FeMo_{0.2}Ni$	5.18	7.39	0.136	−2.474	14.73	0.0415	0.5490	FCC + BCC + σ	[35]
$AlCoCrCuFeNiMo_{0.2}$	5.08	7.77	0.133	−4.47	15.6	0.0125	0.6045	FCC + BCC	[16]
$AlCoCrCuFeNiMo_{0.4}$	5.15	7.72	0.145	−4.2	15.91	0.0257	0.5999	BCC + α	[16]
$AlCoCrCuFeNiMo_{0.6}$	5.21	7.67	0.154	−3.95	16.08	0.0144	0.5924	BCC + α	[16]
$AlCoCrCuFeNiMo_{0.8}$	5.26	7.62	0.162	−3.72	16.16	0.0131	0.5841	BCC + α	[16]
$AlCoCrCuFeNiMo$	5.29	7.57	0.168	−3.51	16.18	0.0130	0.5782	BCC +α	[16]
$CoCrCu_{0.1}Fe_{0.15}NiMo_{1.5}Mn_{0.05}$	4.70	7.64	0.185	−4.61	13.14	0.0092	0.5948	FCC + BCC + μ	[13]
$CoCrCu_{0.1}Fe_{0.15}NiMo_{1.5}Mn_{0.12}$	4.68	7.63	0.189	−4.52	13.44	0.0091	0.6136	FCC + BCC + μ	[13]
$CoCrCu_{0.1}Fe_{0.15}NiMo_{1.5}Mn_{0.3}$	4.64	7.60	0.197	−4.29	13.90	0.0091	0.6456	FCC + BCC + μ	[13]
$CoCrCu_{0.1}FeNiMo$	4.216	7.86	0.159	−3.63	13.92	0.0097	0.7831	FCC + BCC	[33]
$CoCrCu_{0.3}FeNiMo$	4.181	7.98	0.157	−1.83	14.44	0.0096	0.8260	FCC + BCC	[33]
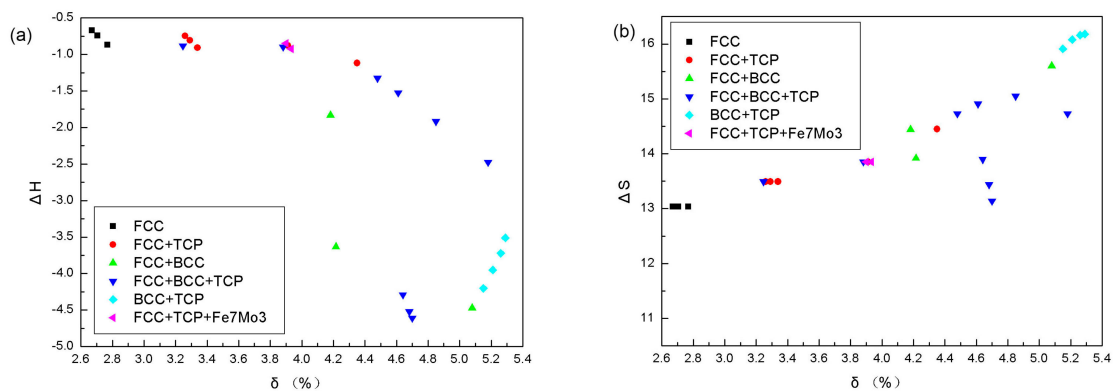
Figure 5. *Cont.*
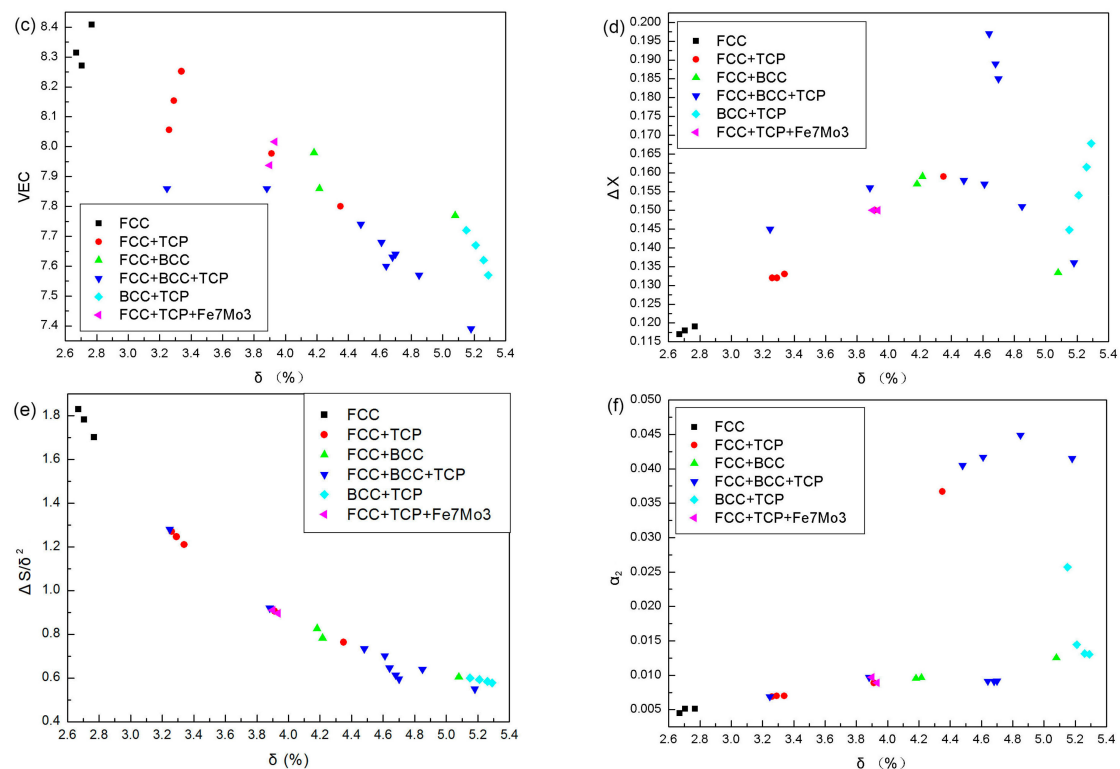
Figure 5. The relationships between parameters and phase structures.

5. Conclusions

Eutectic or dendritic microstructures were observed in as-solidified $CoCrCu_{0.1}FeMoNi$-based HEAs. A fully eutectic microstructure was found in $CoCr_{1.5}Cu_{0.1}FeMo_{0.5}Ni$ and $CoCrCu_{0.1}Fe_{1.2}Mo_{0.8}Ni$ alloys. TCP phases were detected in most of the $CoCrCu_{0.1}FeMoNi$-based HEAs except for the $Co_{1.7}CrCu_{0.1}FeMo_{0.3}Ni$, $CoCrCu_{0.1}Fe_{1.7}Mo_{0.3}Ni$, and $CoCrCu_{0.1}FeMo_{0.3}Ni_{1.7}$ alloys. A simple FCC single-phase solid solution was obtained when the molar ratio of Fe, Co, and Ni was increased to 1.7 at the expense of Mo. This indicated that Fe, Co, and Ni are FCC stabilizers in the $CoCrCu_{0.1}FeMoNi$-based alloy system.

Moreover, a simple FCC structure was found in the alloys with the smallest δ, ΔX, and ΔS values. Conversely, alloys with higher VEC were simple FCC structures, while TCP phases appeared to develop in alloys with decreased VEC. TCP phases were found with large negative ΔH values, with the exception of the $Cu_{0.1}Mo_{0.3}Ni_{0.7}$ alloy. Furthermore, the value of α_2 is smaller when a simple FCC structure is obtained.

For $CoCrCu_{0.1}FeMoNi$-based alloys, the FCC structure was stable when $\delta \leq 2.8$, VEC ≥ 8.27, $\Delta S \leq 13.037$, $\alpha_2 \leq 0.0051$, and $\Delta S/\delta^2 > 1.7$; the mixture of FCC+BCC is favored when $4.1 \leq \delta \leq 4.3$ while the (FCC or/and BCC + IM) mixture is found when $2.8 \leq \delta \leq 4.1$ or $\delta > 4.3$. IM phases are favored when $\Delta X > 0.133$. However, some overlap remained in parameters including VEC, ΔS, α_2, and $\Delta S/\delta^2$. This indicated that these parameters are not sufficient to distinguish (FCC or/and BCC + IM) from (FCC+BCC) phase formation behaviors, and new rules or parameters must be considered for the described system. Moreover, ΔH could not predict phase structures in the current work. In summary, the phase selection behaviors in $CoCrCu_{0.1}FeMoNi$-based HEAs can be well delineated by δ and ΔX.

Author Contributions: Conceptualization, N.L.; Methodology, C.C. and P.Z.; Software, C.C. and X.W; Validation, N.L., C.C., I.C., P.Z. and X.W; Formal Analysis, X.W.; Investigation, N.L. and C.C.; Resources, N.L.; Data Curation, C.C.; Writing-Original Draft Preparation, N.L. and C.C.; Writing-Review & Editing, I.C.; Project Administration, N.L.; Funding Acquisition, N.L.

References

1. Cantor, B.; Chang, I.T.H.; Knight, P.; Vincent, A.J.B. Microstructure development in equiatomic multicomponent alloys. *Mater. Sci. Eng. A* **2004**, *375*, 213–218. [CrossRef]
2. Miracle, D.B.; Senkov, O.N. A critical review of high entropy alloys and related concepts. *Acta Mater.* **2017**, *122*, 488–511. [CrossRef]
3. Gorsse, S.; Miracle, D.B.; Senkov, O.N. Mapping the world of complex concentrated alloys. *Acta Mater.* **2017**, *135*, 177–187. [CrossRef]
4. Senkov, O.N.; Rao, S.; Chaput, K.J.; Woodward, C. Compositional effect on microstructure and properties of NbTiZr-based complex concentrated alloys. *Acta Mater.* **2017**, *122*, 488–511. [CrossRef]
5. Yurchenko, N.Y.; Stepanov, N.D.; Zherebtsov, S.V.; Tikhonovsky, M.A.; Salishchev, G.A. Structure and mechanical properties of B2 ordered refractory AlNbTiVZr$_x$ (x = 0–1.5) high-entropy alloys. *Mater. Sci. Eng. A* **2017**, *704*, 82–90. [CrossRef]
6. Stepanov, N.D.; Shaysultanov, D.G.; Chernichenko, R.S.; Ikornikov, D.M.; Zherebtsov, S.V. Mechanical properties of a new high entropy alloy with a duplex ultra-fine grained structure. *Mater. Sci. Eng. A* **2018**, *728*, 82–90. [CrossRef]
7. Yurchenko, N.Y.; Stepanov, N.D.; Gridneva, A.O.; Mishunin, M.V.; Salishchev, G.A.; Zherebtsov, S.V. Effect of Cr and Zr on phase stability of refractory Al-Cr-Nb-Ti-V-Zr high-entropy alloys. *J. Alloys Compd.* **2018**, *757*, 403–414. [CrossRef]
8. Wang, Z.J.; Guo, S.; Liu, C.T. Phase Selection in High-Entropy Alloys: From Nonequilibrium to Equilibrium. *JOM* **2014**, *66*, 1966–1972. [CrossRef]
9. Lu, Z.P.; Wang, H.; Chen, M.W.; Baker, I.; Yeh, J.W.; Liu, C.T.; Nieh, T.G. An assessment on the future development of high-entropy alloys: Summary from a recent workshop. *Intermetallics* **2015**, *66*, 67–76. [CrossRef]
10. Lu, Y.; Dong, Y.; Guo, S.; Jiang, L.; Kang, H.; Wang, T.; Wen, B.; Wang, Z.; Jie, J.; Cao, Z.; et al. A promising new class of high-entropy alloys: Eutectic high-entropy alloys. *Sci. Rep.* **2014**, *4*, 6200. [CrossRef] [PubMed]
11. Guo, S.; Ng, C.; Liu, C.T. Anomalous solidification microstructures in Co-free Al$_x$CrCuFeNi$_2$ High-Entropy Alloys. *J. Alloys Compd.* **2013**, *557*, 77–81. [CrossRef]
12. Liu, N.; Wu, P.H.; Peng, Z.; Xiang, H.F.; Chen, C.; Wang, X.J.; Zhang, J. Microstructure, phase stability and properties of CoCr$_{0.5}$Cu$_x$Fe$_y$MoNi compositionally complex alloys. *Mater. Sci. Technol.* **2017**, *133*, 210–214. [CrossRef]
13. Wu, P.H.; Peng, Z.; Liu, N.; Niu, M.; Zhu, Z.X.; Wang, X.J. The Effect of Mn Content on the Microstructure and Properties of CoCrCu$_{0.1}$Fe$_{0.15}$Mo$_{1.5}$Mn$_x$Ni near Equiatomic Alloys. *Mater. Trans.* **2016**, *57*, 5–8. [CrossRef]
14. Jiang, L.; Cao, Z.Q.; Jie, J.C.; Zhang, J.J.; Lu, Y.P.; Wang, T.M.; Li, T.J. Effect of Mo and Ni elements on microstructure evolution and mechanism properties of the CoFeNi$_x$VMo$_y$ high entropy alloys. *J. Alloys Compd.* **2015**, *649*, 585–590. [CrossRef]
15. He, F.; Wang, Z.J.; Cheng, P.; Wang, Q.; Li, J.J.; Dang, Y.Y.; Wang, J.C.; Liu, C.T. Designing eutectic high entropy alloys of CoCrFeNiNb$_x$. *J. Alloys Compd.* **2015**, *656*, 284–289. [CrossRef]
16. Zhu, J.M.; Zhang, H.F.; Fu, H.M.; Wang, A.M.; Li, H.; Hu, Z.Q. Microstructures and compressive properties of multicomponent AlCoCrFeNiMo$_x$ alloys. *Mater. Sci. Eng. A* **2010**, *527*, 6975–6979. [CrossRef]
17. Zhu, J.M.; Fu, H.M.; Zhang, H.F.; Wang, A.M.; Li, H.; Hu, Z.Q. Microstructures and compressive properties of multicomponent AlCoCrCuFeNiMo$_x$ alloys. *J. Alloys Compd.* **2010**, *497*, 52–56. [CrossRef]
18. He, F.; Wang, Z.J.; Zhu, M.; Li, J.J.; Dang, Y.Y.; Wang, J.C. The phase stability of Ni$_2$CrFeMo$_x$ multi-principal-component alloys with medium configurational entropy. *Mater. Des.* **2015**, *85*, 1–6. [CrossRef]
19. Hsu, C.Y.; Juan, C.C.; Wang, W.R.; Sheu, T.S.; Chen, S.K.; Yeh, J.W. On the superior hot hardness and softening resistance of AlCoCr$_x$FeMo$_{0.5}$Ni high-entropy alloys. *Mater. Sci. Eng. A* **2011**, *528*, 3581–3588. [CrossRef]
20. Hsu, C.Y.; Sheu, T.S.; Wang, W.R.; Tang, W.Y.; Chen, S.K.; Yeh, J.W. Microstructure and Mechanical Properties of New AlCo$_x$CrFeMo$_{0.5}$Ni High-Entropy Alloys. *Adv. Eng. Mater.* **2010**, *12*, 44–49. [CrossRef]
21. Liu, W.H.; Lu, Z.P.; He, J.Y.; Luan, J.H.; Wang, Z.J.; Liu, B.; Liu, Y.; Chen, M.W.; Liu, C.T. Ductile CoCrFeNiMo$_x$ high entropy alloys strengthened by hard intermetallic phases. *Acta Mater.* **2016**, *116*, 332–342. [CrossRef]
22. Li, X.C.; Dou, D.; Zheng, Z.Y.; Li, J.C. Microstructure and Properties of FeAlCrNiMo$_x$ High-Entropy Alloys. *J. Mater. Eng. Perform.* **2016**, *25*, 2164–2169. [CrossRef]

23. Tian, L.H.; Xiong, W.; Liu, C.; Lu, S.; Fu, M. Microstructure and wear behavior of atmospheric plasma-sprayed AlCoCrFeNiTi high-entropy alloy coating. *J. Mater. Eng. Perform.* **2016**, *25*, 5513–5521. [CrossRef]

24. Zhang, Y.; Zhou, Y.J.; Lin, J.P.; Chen, G.L.; Liaw, P.K. Solid-solution phase formation rules for multi-component alloys. *Adv. Eng. Mater.* **2008**, *10*, 534–538. [CrossRef]

25. Guo, S.; Liu, C.T. Phase stability in high entropy alloys: Formation of solid-solution phase or amorphous phase. *Prog. Nat. Sci.* **2011**, *21*, 433–446. [CrossRef]

26. Zhang, Y.; Yang, X.; Liaw, P.K. Alloy Design and Properties Optimization of High-Entropy Alloys. *JOM* **2012**, *64*, 830–838. [CrossRef]

27. Yang, X.; Zhang, Y. Prediction of high-entropy stabilized solid-solution in multicomponent alloys. *Mater. Chem. Phys.* **2012**, *132*, 233–238. [CrossRef]

28. Yang, X.; Chen, S.Y.; Cotton, J.D.; Zhang, Y. Phase stability of low-density, multiprincipal component alloys containing aluminum, magnesium, and lithium. *JOM* **2014**, *10*, 2009–2020. [CrossRef]

29. Wang, Z.J.; Huang, Y.H.; Yang, Y.; Wang, J.C.; Liu, C.T. Atomic-size effect and solid solubility of multicomponent alloys. *Scr. Mater.* **2015**, *94*, 28–31. [CrossRef]

30. Tsai, M.H.; Tsai, K.Y.; Tsai, C.W.; Lee, C.; Juan, C.C.; Yeh, J.W. Criterion for sigma phase formation in Cr- and V-containing high-entropy alloys. *Mater. Res. Lett.* **2013**, *1*, 207–212. [CrossRef]

31. Dong, Y.; Lu, Y.; Jiang, L.; Wang, T.; Li, T. Effect of electro-negativity on the stability of topologically close-packed phase in high entropy alloys. *Intermetallics* **2014**, *52*, 105–109. [CrossRef]

32. Wang, Z.J.; Qiu, W.F.; Yang, Y.; Liu, C.T. Atomic-size and lattice-distortion effects in newly developed high-entropy alloys with multiple principal elements. *Intermetallics* **2015**, *64*, 63–69. [CrossRef]

33. Wu, P.H.; Liu, N.; Yang, W.; Zhu, Z.X.; Lu, Y.P.; Wang, X.J. Microstructure and Solidification Behavior of Multi-component CoCrCu$_x$FeMoNi High-entropy alloys. *Mater. Sci. Eng. A* **2015**, *642*, 142–149. [CrossRef]

34. Lu, Y.; Jiang, H.; Guo, S.; Wang, T.; Cao, Z.; Li, T. A new strategy to design eutectic high-entropy alloys using mixing enthalpy. *Intermetallics* **2017**, *9*, 124–128. [CrossRef]

35. Wu, P.H. Microstructure and Solidification Behavior of Multi-Component CoCrCuxFeMoNi High-Entropy Alloys. Master's Thesis, Jiangsu University of Science and Technology, Zhenjiang, China, 15 June 2016.

36. Singh, A.K.; Kumar, N.; Dwivedi, A.; Subramaniam, A. A geometrical parameter for the formation of disordered solid solutions in multi-component alloys. *Intermetallics* **2014**, *52*, 105–109. [CrossRef]